Modeling Li-Ion Batteries for Automotive Application: a Trade-Off between Accuracy and Complexity

Davide Cittanti, Alessandro Ferraris, Andrea Airale, Sabina Fiorot, Santo Scavuzzo, Massimiliana Carello
Department of Mechanical and Aerospace Engineering
Politecnico di Torino
Torino, Italy
massimiliana.carello@polito.it

***Abstract* — This paper presents a fast and effective approach to Li-ion battery performance modeling, particularly suited for automotive applications (i.e. HEV, PHEV, BEV). A second-order electrical equivalent circuit model made up by one voltage source, one series resistor and two series RC blocks (dual-polarization model), is here selected as the best trade-off solution for the task, addressing both acceptable levels of accuracy and complexity. While a lithium-iron-phosphate cylindrical battery cell is chosen for the purpose of the study, the presented procedure has broader validity and is mostly independent of Li-ion chemistry and/or cell format. The battery model is parametrized through a low time-consuming current pulse test, performed during both charging and discharging, at different state of charge levels. The temperature and load-current effects on the battery performance are not considered for simplicity and lightness of the presented model. Validation is carried out by comparing measured and simulated results during the dynamic current pulse test, showing a high level of agreement between the two.**

***Keywords* — lithium-ion battery, battery model, electrical equivalent circuit (EEC) model, dual-polarization (DP) model, current pulse test, parameter extraction, electric vehicles.**

I. Introduction

Lithium-ion (Li-ion) batteries have gathered great scientific and market attention during the last two decades, in response to an increasing demand in portable electronics: high energy density (both gravimetric and volumetric), high efficiency, low self-discharge and relatively long life have been the major advantages of this technology in respect to nickel-cadmium. However, even though battery cell employment in consumer electronics is rapidly approaching market saturation, a steep increase in overall Li-ion battery demand is expected in the recent years to come, since the technology is rapidly becoming attractive for other sectors, such as stationary power storage, hybrid and electric vehicles, space power systems and back-up (UPS) applications. The biggest issues with lithium-ion battery cells, such as safety, operating temperature range, and cost, are quickly being addressed by technology advancements and mass production. An overview and future prospect regarding different Li-ion chemistries, along with their most suitable application, is shown in [1], [2].

The automotive sector, above all, is now on the edge of a drastic shift, since international regulations on fuel consumption and carbon emissions are becoming increasingly binding and, therefore, manufacturing common gasoline or diesel powered vehicles may soon no longer be allowed. In order to meet pollution restrictions, researchers are developing and deploying vehicles with an increasing level of electric hybridization, from hybrid electric vehicles (HEVs) [3], to plug-in hybrid electric vehicles (PHEVs) [4], [5] and eventually to pure electric vehicles (EVs). This phenomenon is acting as a strong driving force for Li-ion battery technology, both from a scientific development and a cost reduction point of view. While automotive battery requirements vary depending on drivetrain power and level of hybridization of the specific vehicle considered, commonly desired characteristics are high energy and power density, high level of safety and reliability, high life cycle number (which translates in long vehicle mileage) and lowest possible cost. These properties are mostly embodied by lithium-iron-phosphate ($LiFePO_4$) battery chemistry: while it is not the most energy dense Li-ion cathode technology, it shows exceptional stability (intrinsic safety, long life cycles), high power capability during both charge and discharge and low material cost [2], [6], [7].

Since lithium-ion battery performance highly depends on the operating conditions, such as the state of charge (SOC), temperature and load current, it is non-trivial to understand how battery cells will behave in a certain application. In order to optimize system-level design and energy management control strategies, this knowledge is essential: battery performance modeling and extensive battery cell characterization allow to accurately predict battery terminal current and voltage (I-V behavior) in most conditions. Accurate simulations also allow avoiding a lot of real-world tests on the battery itself, thus reducing required time and cost. Furthermore, battery models are often needed for real-time applications, such as in battery management systems (BMS), which monitor and control Li-ion battery cells when grouped and wired into packs. The main tasks of a BMS are to balance the battery pack (i.e. keeping the cells at the same SOC level) and to communicate its energy and power availability to the rest of the system. To execute these tasks in an effective way, an accurate battery model, able to estimate each battery cell's SOC and state of health (SOH) from its terminal voltage and load-current history, must be implemented in the BMS on-line control strategy.

A large number of battery cell model types are reported in literature, but the most suitable for system-level design and real-time application are definitely electrical models, also known as electrical equivalent circuits (EEC). Two main kinds of EECs exist [8]–[11]: impedance-based models and Thévenin-based models. Impedance-based models usually contain a complex network of circuit elements and specific impedance blocks (such as the constant-phase Warburg element) to fit experimental impedance spectra, extracted by electrochemical impedance spectroscopy (EIS) tests in the frequency domain [12], [13]. Since the EIS test procedure requires specific instrumentation and the fitting process is complex and non-intuitive, impedance-based models are not commonly adopted in practice. Thévenin-based models, on the contrary, are easier to work with, as they are normally made up by a series of a voltage source, a resistor and a set of parallel RC blocks: the parameter values are fitted on battery voltage responses to load current pulses in the time domain [9]. These models are particularly attractive, due to their simplicity, easiness of comprehension and standard test instrumentation requirement: they are therefore the most adopted models.

Specifically, battery models for automotive application must have the best trade-off between simulation accuracy, computational complexity and parametrization effort. In general, the higher the model fidelity, the more effort will be required from both testing (time-consuming and expensive) and computing. Since the automotive field requires light and efficient models which must not sacrifice accuracy, both for system-level simulation (e.g. drivetrain electrification) and for real-time applications (e.g. BMS), the Thévenin-based EEC models represent the best choice. Battery model parameters can be easily extracted from pulse charging/discharging cell responses in different operating conditions, using standard laboratory equipment (e.g. power supplies, electronic loads, multimeters, etc.) in a short time period [14]. Furthermore, it is important to mention that accuracy and complexity of a Thévenin-based model both increase with the number of RC blocks adopted, as shown in [15].

The scope of this paper is to present an automotive-specific battery model, valid for a generic lithium-ion battery chemistry, highlighting its strengths and weaknesses during the battery cell testing, parameter extraction and simulation phases. The goal of the work is to provide automotive designers and powertrain engineers a complete tool to test, extract and model the battery behavior under different operating conditions: knowledge which may be used for system-level design or real-time control logics.

This paper is organized as follows. In section II, a Thévenin-based EEC model for electrified vehicle applications (HEV, PHEV, EV) is proposed and its choice is justified. Section III describes the battery cell chosen for this work and the experimental setup utilized to perform the cell characterization tests, which are presented in section IV. Section V illustrates the battery model parameter extraction procedure, while section VI shows a comparison between measured and simulated data, to provide validation of the proposed model. Finally, section VII concludes this paper.

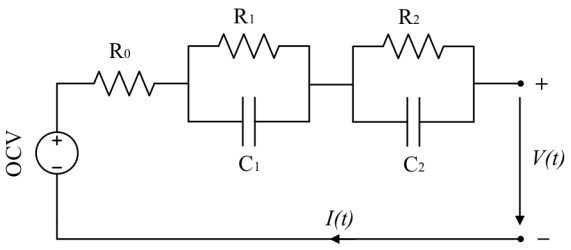

Fig. 1. Dual polarization model.

II. Battery Performance Model

Even restricting the battery model choice to the Thévenin-based EEC models (for the reasons illustrated in the previous section), a wide range of alternatives still exists among them: an overview of these models and their performance comparison is available at [16]–[18]. Thévenin-based models differ mainly in the number of RC parallel pairs they possess, which affect both their accuracy and complexity [15]: the most common models found in literature present one RC block, as in [19]–[22], two RC blocks, as in [10], [11], [23]–[28], three RC blocks, as in [29] and a more generic N RC blocks, as in [30], [31].

Given the relatively low complexity required by automotive system-level simulations and on-line control algorithms, no more than two RC blocks can be adopted for most applications. Furthermore, since one single RC pair is not capable of accurately modeling both fast and slow dynamics (an essential feature for automotive applications), the second-order Thévenin-based EEC model is chosen for the purpose of this paper. This equivalent circuit model, shown in Fig. 1, is made up by a voltage source in series with a resistor and two RC blocks. It is also known as double polarization (DP) model, since the two RC pairs normally represent the behavior of two different dynamical processes taking place inside the battery [11], [22], [28], [32]: the activation polarization and the concentration polarization. The activation polarization, or charge-transfer polarization, represents the voltage involved in increasing the rate of the chemical reactions, or, in other words, the voltage needed to overcome the activation barrier: this phenomenon is the fastest between the two and is thus fitted by the smaller time constant RC block (R_1C_1). The concentration polarization, also known as diffusion or mass-transport polarization, represents the voltage involved in the concentration gradients of the charge carriers in the electrolyte: this is the slowest between the two phenomena and is thus fitted by the larger time constant RC block (R_2C_2). The series resistor R_0 represents the ohmic resistance of the battery cell, which is made up by different contributions belonging to the cell connectors, the current collectors, the electrolyte and the active materials. Finally, the voltage source represents the open circuit voltage (OCV), also referred as the cell terminal voltage in thermodynamic equilibrium conditions.

It must be mentioned that all the presented model parameters highly depend on operating conditions. OCV and R_0 mostly depend on SOC and temperature, while resistors and capacitors belonging to the RC blocks also depend on load

current (and its direction). This means that high-level accuracy models must consider all these dependencies, by extensively characterizing the battery cell, which is expensive and time-consuming at least. In order not to overcomplicate the model and the characterization procedure, while maintaining a fast and efficient approach, some choices have been made for the purpose of this work: temperature and load current effects on battery performance have been neglected, restraining the parameter dependencies to state of charge and current direction. As a matter of fact, avoiding the load current dependency of the parameters does not greatly affect the model accuracy, while neglecting their temperature dependency definitely impacts on the model fidelity. However, implementing temperature-dependent circuit components would also require the realization of a parallel running thermal model to estimate the battery cell temperature during the simulation, which would worsen the computational burden.

The SOC dependency of the equivalent circuit elements is implemented in look-up table form, thus a running SOC calculator block is needed inside the model. An algorithm integrates the instantaneous battery load current and computes the SOC through its definition:

$$SOC(t) = SOC(0) - 100\frac{\int_0^t I(t)dt}{C\ 3600} \quad (1)$$

where $SOC(t)$ is the battery state of charge in percentage form, $SOC(0)$ the initial state of charge, $I(t)$ the instantaneous load current in A and C is the battery cell capacity in Ah. The SOC information thus exits the calculator block and gets fed to the equivalent circuit parameter look-up tables: the whole model is easily implemented in MATLAB/Simulink environment.

III. Experimental Setup

The characterization tests are performed on a specific $LiFePO_4$ cell from A123, the ANR26650M1-B cylindrical model [33]: its main parameters are reported in TABLE I. The experimental setup is shown in Fig. 2 and is made up by a Solartron Analytical 1470 battery cell tester [34], connected to the battery cells under test through power wires and directly communicating with a computer through GPIB interface. The tester has 8 separated test channels available, each capable of withstanding 15 V and carrying 4 A (either in charge or discharge), but more channels can be wired in parallel to carry higher currents. Neither of the tests here presented requires parallel configurations, since the absolute value of the current is never greater than 4 A, therefore the battery cells under test are wired to separate channels of the testing device. The Solartron Analytical 1470 can be programmed through a software interface to charge/discharge the connected battery cells with user-defined dynamical current or voltage profiles. This allows to perform all the test procedures presented in the following section. It must be said that the tests have been performed on three cells of the same type to reach a minimal statistical relevance, however, the behavior under test and the set of extracted EEC parameters belonging to only one cell will be shown, for clarity reasons.

TABLE I. Battery Datasheet Parameters

Property	Value
Nominal capacity	2.5 Ah
Nominal voltage	3.3 V
Max. voltage	3.6 V
Min. voltage	2.5 V
Max. discharge current	70 A (21-C)
Max. charge current	10 A (4-C)
Operating temperature	-30 °C to 55°C
Cycle life	> 1000 cycles

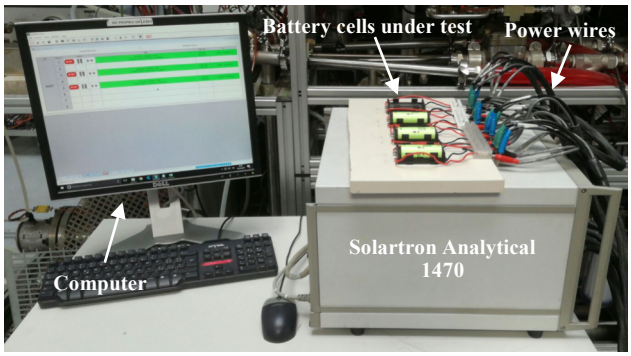

Fig. 2. Overview of the laboratory test setup.

IV. Characterization Procedure

The battery cells are characterized by a set of subsequent tests, illustrated in Fig. 3, which aim to collect the necessary data to parametrize the presented equivalent circuit model.

A. Preconditioning test

The preconditioning test here implemented is made up by three full charge/discharge cycles at 0.5C (i.e. 1.25 A) carried out at ambient temperature. A 90-minute rest is undertaken after either every full charge or discharge. The total time required by this test is roughly 24 hours.

B. Capacity test

The capacity of a battery cell (i.e. the total charge that the cell can provide during a full discharge) represents one of its most important parameters, since it not only provides an indication of the battery energy content, but its value is also necessary to define the state of charge variable, as shown in (1).

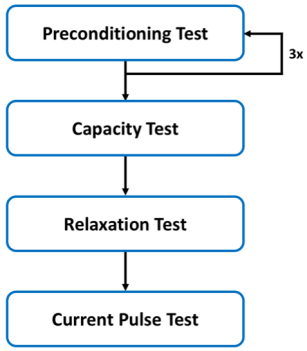

Fig. 3. Battery cell characterization flow chart.

A nominal capacity value is always provided by the manufacturer inside the battery cell datasheet (i.e. TABLE I), however, since it represents a worst-case estimate, a test should be performed to estimate a more reasonable value to be employed inside the cell model.

Battery capacity normally depends on the discharge current at which the test is performed, following Peukert's law:

$$C_{1C} = I^k t \quad (2)$$

where C_{1C} is the capacity of the cell measured during a 1C discharge, I is the discharge current, t is the time required by the discharge and k is the Peukert's coefficient (≥ 1). Since lithium-ion batteries show a Peukert's coefficient value very close to 1 [6], the total charge that can be extracted from the cell is not significantly dependent on the current value. However, the load current largely affects the battery terminal voltage drop and, in order to avoid hitting prematurely the lower discharging threshold voltage (i.e. 2.5 V), an effective capacity measurement should be performed at low current rates. This paper will consider a unique value of capacitance (independent on the charging/discharging current rate) extracted at C/5 (i.e. 0.5 A).

This test can be performed both by charging or discharging the battery: in the first case a constant current (CC) charge at C/5 is applied until the upper voltage threshold is reached (i.e. 3.6 V), thus a constant voltage (CV) procedure holds the voltage at its maximum until the current falls below C/200 (i.e. 0.0125 A); in the second case only a constant current discharge at C/5 is applied, until the lower voltage threshold (i.e. 2.5 V) is reached. The voltage and current waveforms are shown in Fig. 4: a capacity value of approximatively 2650 mAh is extracted. The time required by the CC discharging test is roughly 5 hours.

C. Relaxation test

The relaxation test should provide a comprehensive view of the battery cell dynamics: the aim of this test is to show the order of magnitude of the time constants involved in the battery dynamical response. The cell is discharged with a constant current value of 2.5 A until 50% SOC is reached. The current is then interrupted and the voltage is measured during a 20-hour relaxation period, as in Fig. 5(a).

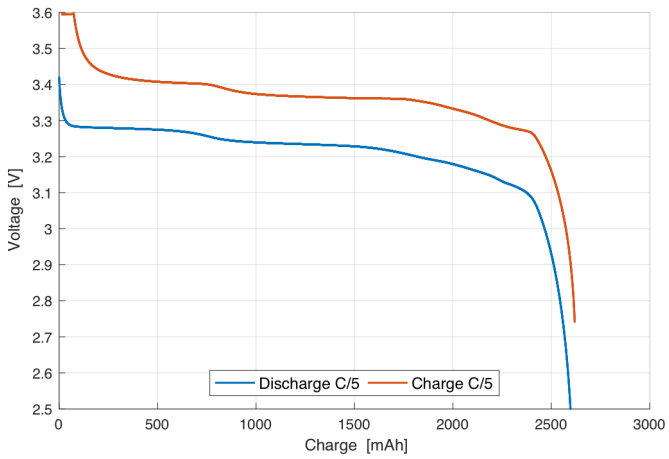

Fig. 4. Battery capacity test.

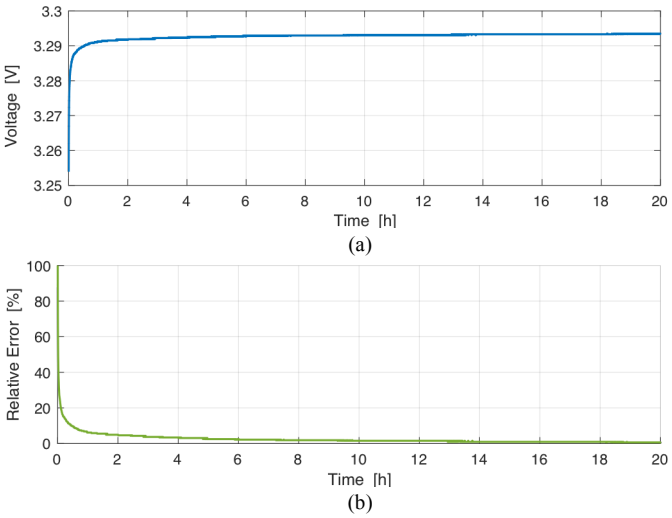

Fig. 5. Voltage relaxation (a) and voltage relative error (b)

The complete battery cell characterization is a highly time-consuming process, mostly due to the numerous and recurring relaxation periods during the current pulse test (presented in the following section), therefore the time length of these periods must be chosen carefully. Long relaxation times provide accurate OCV data but have a considerable impact on the overall test time, thus a compromise must be accomplished. The relative error made by cutting off the relaxation at a certain time instant can be expressed as:

$$\varepsilon_r(t) = \frac{OCV - V(t)}{OCV - V(0)} \quad (3)$$

where OCV is the open circuit voltage (the last voltage value of the relaxation period), while $V(t)$ and $V(0)$ are the instantaneous voltage and the initial voltage value respectively. The voltage relative error is shown in percentage form in Fig. 5(b): it can be noticed that the greatest amount of the error (more than 90%) falls during the first hour of relaxation.

D. Current pulse test

This test allows the proper characterization of the EEC model by soliciting the battery with charging/discharging current pulses while observing its voltage response. Furthermore, to fully parametrize the equivalent circuit elements, pulses must be performed across the whole battery SOC range. The test procedure implemented in this work is shown in Fig. 6 and consists of three main parts:

1. Series of 1C discharging current pulses (i.e. 2.5 A) separated by 10-minute rest periods in between. Each pulse discharges 5% of the battery cell SOC, until the lower threshold voltage is reached (i.e. 2.5 V) and a constant voltage discharging procedure is applied to fully discharge the cell.
2. 10-hour rest period; the cell approaches thermodynamic equilibrium and chemical hysteresis effects are reduced.
3. Series of 1C charging pulses separated by 10-minute rest periods in between. Each pulse charges 5% of the battery cell SOC, until the upper voltage threshold is reached (i.e. 3.6 V) and a constant voltage charging procedure is applied to fully charge the cell.

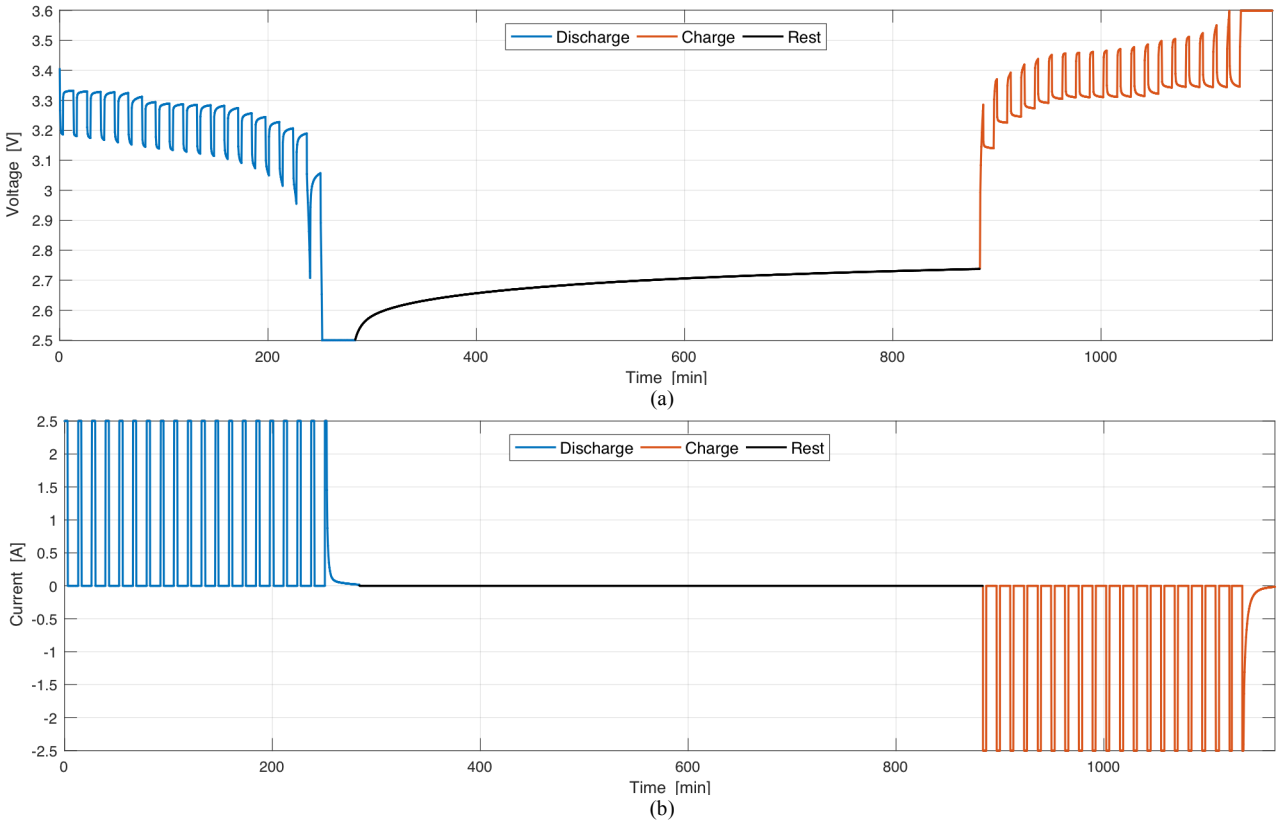

Fig. 6. Current pulse test: voltage (a) and current (b) waveforms.

It is easy to see how the relaxation periods between pulses account for the most part of the overall test time: the here-implemented procedure is quite rapid, as the whole dynamic characterization test can be carried out in less than 24 hours. However, this choice has undoubtedly its drawbacks, since the model will only be capable of predicting dynamics of higher or same order of the test relaxation period: slow chemistry-related dynamical phenomena will not be modeled in this case. Moreover, low relaxation times directly translate in low OCV accuracy, since the voltage cannot reach its stationary condition (thermodynamic equilibrium), as explained before

V. Parameter Extraction

The model parameter extraction process is based on the current pulse test and is well explained in [9], [26]: the parameter values are obtained from the short rest periods subsequent to the current pulses, since the battery SOC remains unchanged during these phases. A highlight of a single voltage relaxation event is shown in Fig. 7.

The first extracted parameter is the OCV, obtained as the last voltage value at the end of the relaxation: the larger the relaxation period, the more accurate will be the extracted OCV value. The R_0 value is then acquired from the sudden voltage variation V_0 following the current pulse end ΔI:

$$R_0 = \frac{V_0}{\Delta I} \tag{4}$$

Finally, the remaining parameters are obtained by curve-fitting the remaining part of the voltage response $V_1(t) + V_2(t)$, recalling that the double-RC equivalent circuit model response has the following form:

$$V(t) = OCV - V_1 e^{-t/\tau_1} - V_2 e^{-t/\tau_2} \tag{5}$$

The fitting process is carried out in MATLAB environment, using a bounded-parameter least-square algorithm, and V_1, τ_1, V_2, τ_2 are thus extracted. Their relationship with the model equivalent circuit parameters is the following:

$$R_i = \frac{V_i}{\Delta I} \tag{6}$$

$$C_i = \frac{\tau_i}{R_i} \tag{7}$$

R_1, C_1, R_2, C_2 are therefore obtained.

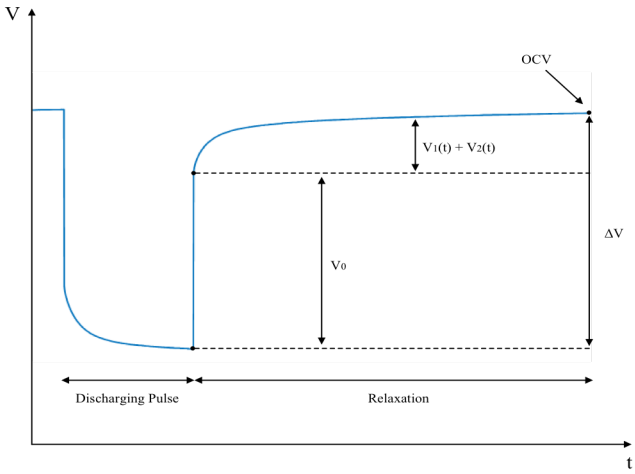

Fig. 7. Highlight of the parameter extraction procedure for a discharging pulse.

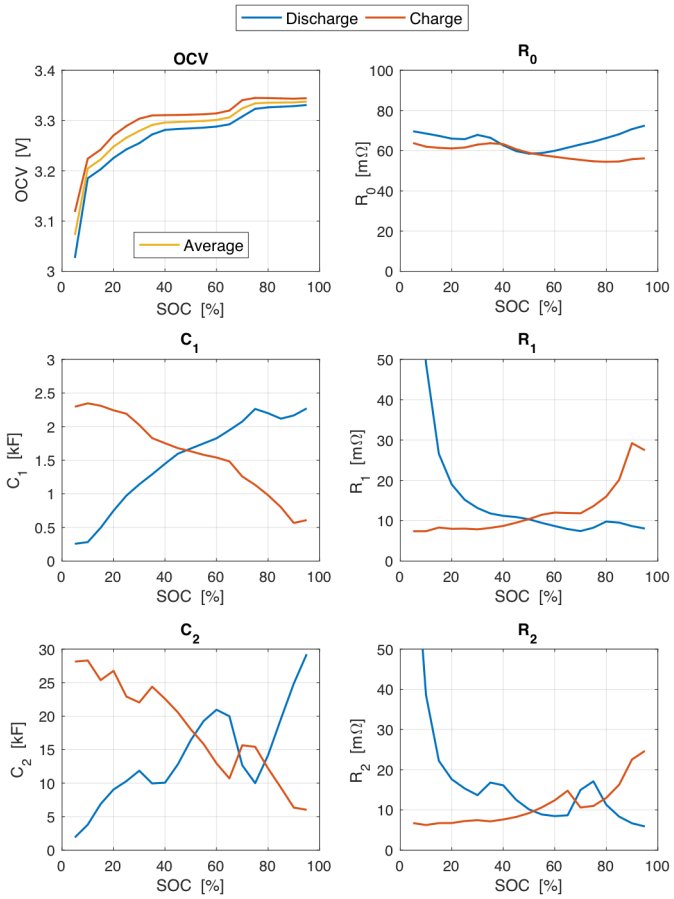

Fig. 8. Extracted equivalent circuit model parameters.

The presented procedure is performed both for the pulse discharging and pulse charging tests: the extracted parameter datasets are only available between 5% and 95% SOC (due to the nature of the test itself) and are shown in Fig. 8. The OCV shape is noticeably different between charging and discharging and the two curves show a roughly constant offset: this is mostly due to the limited relaxation time of the test procedure. In this work, the battery hysteresis effects are neglected, since a very time-consuming experiment would be needed to highlight them: an average value between the charging and discharging OCV is therefore used for the modeling purpose. R_0 shows an approximately constant behavior over the whole SOC range, since the ohmic resistance of the cell only depends on temperature. Furthermore, while time constants τ_1 and τ_2 result nearly independent on SOC, the respective equivalent resistors and capacitors consistently change in value towards the edges of the SOC range. Resistance values increase in discharge towards 0% SOC and in charge towards 100% SOC: this is mainly because, in these regions, both activation and concentration polarization phenomena increase their impact on the battery terminal voltage.

VI. Model Validation

The model validation process is carried out by comparing the measured and simulated waveforms during the current pulse test, both in discharging and charging (Fig. 9). It must be mentioned that the comparison is only performed between 5% and 95% SOC values, in agreement with the model parameter set availability.

The voltage absolute error is shown in Fig. 10, defined as the difference between the measured and the simulated voltage:

$$\varepsilon_{abs}(t) = V_{meas}(t) - V_{sim}(t) \tag{8}$$

A general high fidelity level is observed since the absolute error module lies below 10 mV along most of the test procedure: a considerable increase in the error value is seen towards the end of the test, both in charge and in discharge. This is mostly due to the rapidly increasing cell resistance (R_1 and R_2) while approaching the SOC edges, as shown in Fig. 8: the model parameter discretization becomes insufficient to precisely predict the battery behavior.

While the maximum absolute error hits 88 mV (in the pulse discharging test), a better indicator of the overall model fidelity may be provided by the root mean square error (RMSE):

$$RMSE = \sqrt{\frac{1}{T}\int_0^T [V_{meas}(t) - V_{sim}(t)]^2\, dt} \tag{9}$$

where T is the considered time period. The calculated global RMSE is 5.7 mV.

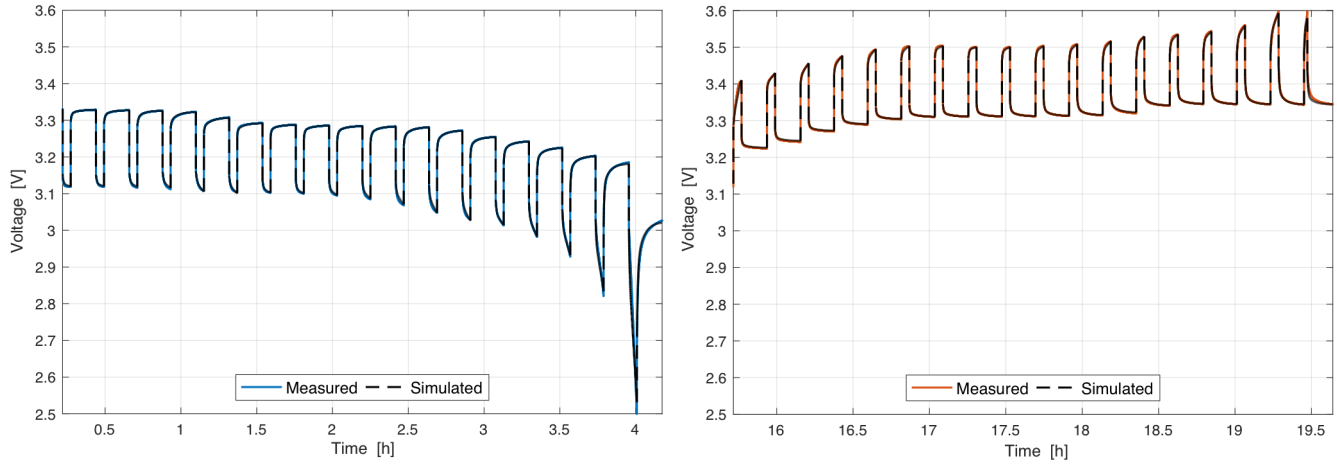

Fig. 9. Comparison between measured and simulated waveforms: discharge (a) and charge (b).

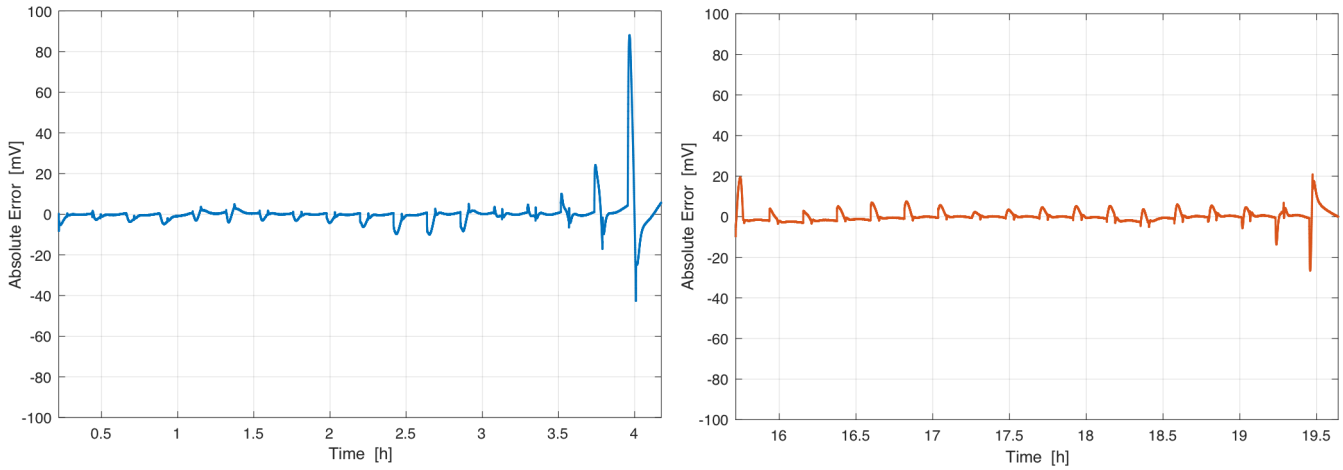

(a) (b)

Fig. 10. Absolute error (in mV) between measured and simulated results: discharge (a) and charge (b).

It should finally be noted that the model better behaves during the relaxation period since the equivalent circuit parameters have been extracted during this phase.

VII. Conclusions

A battery performance modeling approach, mostly suited for automotive applications, is presented in this paper. The scope is to provide a comprehensible and rapid tool for automotive designers and powertrain engineers to model and parametrize battery cells in a time and cost-effective way, without sacrificing a certain level of dynamical precision. A trade-off between accuracy, computational complexity and parametrization effort is achieved, by selecting a double-RC equivalent circuit model and performing a fast and effective set of characterization tests. A final comparison between measured and simulated results validates the performance model, showing a high level of fidelity: the voltage prediction error lies below 10 mV in most of the battery operating SOC range, resulting in an overall RMSE value of 5.7 mV.

Since no tests have been performed to evaluate the battery cell performance dependency on temperature and current rate, the presented model is clearly limited in its predictive capabilities outside the narrow set of extracted parameters. The enhancement of this parameter set will be the object of the authors' future work, in order to extend the model validity to a broader set of operating conditions, while necessarily accepting more expensive and time-consuming testing. The model real-time implementation, coupled with an extended Kalman filter for SOC estimation, will also be the object of future study.

Acknowledgment

Authors want to acknowledge IEHV-Polito research group and Hysylab for providing instrumentation and facilities. Special thanks to Eng. M. Fausone for his helpful advice.

References

[1] B. Scrosati and J. Garche, "Lithium batteries: Status, prospects and future," *J. Power Sources*, vol. 195, no. 9, pp. 2419–2430, May 2010.

[2] A. I. Stan, M. Świerczyński, D. I. Stroe, R. Teodorescu, and S. J. Andreasen, "Lithium ion battery chemistries from renewable energy storage to automotive and back-up power applications - An overview," in *2014 International Conference on Optimization of Electrical and Electronic Equipment (OPTIM)*, 2014, pp. 713–720.

[3] M. Carello, N. Filippo, and R. d'Ippolito, "Performance Optimization for the XAM Hybrid Electric Vehicle Prototype," in *SAE Technical Paper Series*, 2012.

[4] M. Carello, A. Airale, A. Ferraris, and A. Messana, "XAM 2.0: from Student Competition to Professional Challenge," *Comput.-Aided Des. Appl.*, vol. 11, no. sup1, pp. S61–S67, May 2014.

[5] M. Carello, A. Ferraris, A. Airale, and F. Fuentes, "City Vehicle XAM 2.0: Design and Optimization of its Plug-In E-REV Powertrain," in *SAE Technical Paper Series*, 2014.

[6] N. Omar *et al.*, "Evaluation of performance characteristics of various lithium-ion batteries for use in BEV application," in *2010 IEEE Vehicle Power and Propulsion Conference*, 2010, pp. 1–6.

[7] F. P. Tredeau and Z. M. Salameh, "Evaluation of Lithium iron phosphate batteries for electric vehicles application," in *2009 IEEE Vehicle Power and Propulsion Conference*, 2009, pp. 1266–1270.

[8] A. Seaman, T.-S. Dao, and J. McPhee, "A survey of mathematics-based equivalent-circuit and electrochemical battery models for hybrid and electric vehicle simulation," *J. Power Sources*, vol. 256, pp. 410–423, Jun. 2014.

[9] A. Hentunen, T. Lehmuspelto, and J. Suomela, "Time-Domain Parameter Extraction Method for Thevenin-Equivalent Circuit Battery Models," *IEEE Trans. Energy Convers.*, vol. 29, no. 3, pp. 558–566, Sep. 2014.

[10] M. Chen and G. A. Rincon-Mora, "Accurate electrical battery model capable of predicting runtime and I-V performance," *IEEE Trans. Energy Convers.*, vol. 21, no. 2, pp. 504–511, Jun. 2006.

[11] L. Lam, P. Bauer, and E. Kelder, "A practical circuit-based model for Li-ion battery cells in electric vehicle applications," in *2011 IEEE 33rd International Telecommunications Energy Conference (INTELEC)*, 2011, pp. 1–9.

[12] D. Andre, M. Meiler, K. Steiner, C. Wimmer, T. Soczka-Guth, and D. U. Sauer, "Characterization of high-power lithium-ion batteries by electrochemical impedance spectroscopy. I. Experimental investigation," *J. Power Sources*, vol. 196, no. 12, pp. 5334–5341, Jun. 2011.

[13] D. Andre, M. Meiler, K. Steiner, H. Walz, T. Soczka-Guth, and D. U. Sauer, "Characterization of high-power lithium-ion batteries by electrochemical impedance spectroscopy. II: Modelling," *J. Power Sources*, vol. 196, no. 12, pp. 5349–5356, Jun. 2011.

[14] S. Abu-Sharkh and D. Doerffel, "Rapid test and non-linear model characterisation of solid-state lithium-ion batteries," *J. Power Sources*, vol. 130, no. 1–2, pp. 266–274, May 2004.

[15] H. Zhang and M.-Y. Chow, "Comprehensive dynamic battery modeling for PHEV applications," in *IEEE PES General Meeting*, 2010, pp. 1–6.

[16] H. He, R. Xiong, H. Guo, and S. Li, "Comparison study on the battery models used for the energy management of batteries in electric vehicles," *Energy Convers. Manag.*, vol. 64, pp. 113–121, Dec. 2012.

[17] X. Hu, S. Li, and H. Peng, "A comparative study of equivalent circuit models for Li-ion batteries," *J. Power Sources*, vol. 198, pp. 359–367, Jan. 2012.

[18] M. Einhorn, F. V. Conte, C. Kral, and J. Fleig, "Comparison, Selection, and Parameterization of Electrical Battery Models for Automotive Applications," *IEEE Trans. Power Electron.*, vol. 28, no. 3, pp. 1429–1437, Mar. 2013.

[19] T. Huria, M. Ceraolo, J. Gazzarri, and R. Jackey, "High fidelity electrical model with thermal dependence for characterization and simulation of high power lithium battery cells," in *2012 IEEE International Electric Vehicle Conference*, 2012, pp. 1–8.

[20] L. Gao, S. Liu, and R. A. Dougal, "Dynamic lithium-ion battery model for system simulation," *IEEE Trans. Compon. Packag. Technol.*, vol. 25, no. 3, pp. 495–505, Sep. 2002.

[21] F. Baronti, G. Fantechi, E. Leonardi, R. Roncella, and R. Saletti, "Enhanced model for Lithium-Polymer cells including temperature effects," in *IECON 2010 - 36th Annual Conference on IEEE Industrial Electronics Society*, 2010, pp. 2329–2333.

[22] G. Aurilio *et al.*, "A battery equivalent-circuit model and an advanced technique for parameter estimation," in *2015 IEEE International Instrumentation and Measurement Technology Conference (I2MTC) Proceedings*, 2015, pp. 1705–1710.

[23] J. Li and M. S. Mazzola, "Accurate battery pack modeling for automotive applications," *J. Power Sources*, vol. 237, pp. 215–228, Sep. 2013.

[24] W. Y. Low, J. A. Aziz, N. R. N. Idris, and R. Saidur, "Electrical model to predict current–voltage behaviours of lithium ferro phosphate batteries using a transient response correction method," *J. Power Sources*, vol. 221, pp. 201–209, Jan. 2013.

[25] B. Schweighofer, K. M. Raab, and G. Brasseur, "Modeling of high power automotive batteries by the use of an automated test system," *IEEE Trans. Instrum. Meas.*, vol. 52, no. 4, pp. 1087–1091, Aug. 2003.

[26] T. Hu, B. Zanchi, and J. Zhao, "Simple Analytical Method for Determining Parameters of Discharging Batteries," *IEEE Trans. Energy Convers.*, vol. 26, no. 3, pp. 787–798, Sep. 2011.

[27] T. Kim and W. Qiao, "A Hybrid Battery Model Capable of Capturing Dynamic Circuit Characteristics and Nonlinear Capacity Effects," *IEEE Trans. Energy Convers.*, vol. 26, no. 4, pp. 1172–1180, Dec. 2011.

[28] K. Li and K. J. Tseng, "An equivalent circuit model for Li-ion batteries used in energy storage systems in building environment," in *2016 IEEE Innovative Smart Grid Technologies - Asia (ISGT-Asia)*, 2016, pp. 504–510.

[29] L. H. Saw, Y. Ye, and A. A. O. Tay, "Electro-thermal characterization of Lithium Iron Phosphate cell with equivalent circuit modeling," *Energy Convers. Manag.*, vol. 87, pp. 367–377, Nov. 2014.

[30] Y. Hu, S. Yurkovich, Y. Guezennec, and B. J. Yurkovich, "Electro-thermal battery model identification for automotive applications," *J. Power Sources*, vol. 196, no. 1, pp. 449–457, Jan. 2011.

[31] K. S. Hariharan and V. Senthil Kumar, "A nonlinear equivalent circuit model for lithium ion cells," *J. Power Sources*, vol. 222, pp. 210–217, Jan. 2013.

[32] H. He, R. Xiong, X. Zhang, F. Sun, and J. Fan, "State-of-Charge Estimation of the Lithium-Ion Battery Using an Adaptive Extended Kalman Filter Based on an Improved Thevenin Model," *IEEE Trans. Veh. Technol.*, vol. 60, no. 4, pp. 1461–1469, May 2011.

[33] A123 Systems, "Nanophosphate® High Power Lithium Ion Cell." ANR26650M1-B datasheet, 2011.

[34] Solartron Analytical, "Solartron CellTest® System." 1470E Specification Datasheet, 2015.